Batf3 maintains *Irf8* autoactivation for commitment of a CD8α+ cDC clonogenic progenitor

Gary E. Grajales-Reyes[1], **Arifumi Iwata**[1], **Jörn Albring**[2], **Xiaodi Wu**[1], **Roxane Tussiwand**[1,3], **KC Wumesh**[1], **Nicole M. Kretzer**[1], **Carlos G. Briseño**[1], **Vivek Durai**[1], **Prachi Bagadia**[1], **Malay Haldar**[1], **Jörg Schönheit**[4], **Frank Rosenbauer**[5], **Theresa L. Murphy**[1], and **Kenneth M. Murphy**[1,6,*]

[1]Department of Pathology and Immunology, Washington University School of Medicine, St. Louis, MO 63110, USA [2]Department of Medicine A, Hematology and Oncology, University of Muenster, 48149 Muenster, Germany [3]Department of Biomedicine, University of Basel, Basel, Switzerland [4]Institute of Biomaterial Science and Berlin-Brandenburg Center for Regenerative Therapies (BCRT), Helmholtz-Center Geesthacht, Teltow, Germany [5]Institute of Molecular Tumor Biology, University of Münster, 48149 Münster, Germany [6]Howard Hughes Medical Institute, Washington University School of Medicine, St. Louis, MO 63110, USA

Abstract

The transcription factors Batf3 and IRF8 are required for development of CD8α+ conventional dendritic cells (cDCs), but the basis for their actions was unclear. Here, we identify two novel *Zbtb46*+ progenitors that separately generate CD8α+ and CD4+ cDCs and arise directly from the common DC progenitor (CDP). *Irf8* expression in the CDP depends on prior PU.1-dependent autoactivation, and specification of pre-CD8 DC progenitors requires IRF8 but not Batf3. However, upon pre-CD8 DC specification, *Irf8* autoactivation becomes Batf3-dependent at a CD8α+ cDC-specific enhancer containing multiple AP1-IRF composite elements (AICEs) within the *Irf8* superenhancer. CDPs from *Batf3*−/− mice that specify toward pre-CD8 DCs fail to complete CD8α+ cDC development due to decay of *Irf8* autoactivation, and divert to the CD4+ cDC lineage.

Introduction

Individual dendritic cell (DC) lineages have non-redundant roles in defense against pathogens[1]. Plasmacytoid DCs (pDCs) produce type I IFNs to limit viral infections[2] but are limited in presenting antigen to T cells[3]. The two 'classical' DC (cDC) lineages, represented by splenic CD8α+ DCs and CD4+ DCs[4], selectively express IRF8 or IRF4, respectively[5,6].

*To whom correspondence should be addressed: Phone 314-362-2009, Fax 314-747-4888, kmurphy@wustl.edu.

IRF8[+] cDCs function *in vivo* in cross-presentation to CD8 T cells and induction of IL-12-dependent T_H1 responses[7,8], while IRF4^{+} cDCs function in promoting T_H17 and T_H2 immune responses[9–11]. Both *in vivo* and in FLT3L-treated BM cultures IRF8^{+} cDCs can be identified as CD24^{+} CD172a^{−} and IRF4^{+} cDCs can be identified as CD24^{−} CD172a^{+}. Below we refer to CD8α^{+} IRF8^{+} DCs as CD24^{+} DCs and CD4^{+} IRF4^{+} DCs as CD172a^{+} cDCs.

Several transcription factors control DC development from the BM-resident common DC progenitor (CDP)[12–14]. IRF8 is expressed by and required for the development of both pDCs and CD24^{+} DCs[6,15–17]. Reportedly, IRF8 binds its own promoter in a macrophage cell line[18] and may be regulated by a positive autoregulatory loop in pDCs[19]. In contrast, IRF4 is required in the CD172a^{+} DC lineage[20]. E2-2 is expressed by pDCs and required for their development[3,21], while Id2, an inhibitor class of basic helix-loop-helix (bHLH) transcription factor, is expressed by both cDC subsets but is only required for development of CD24^{+} cDCs[22–24].

Batf3-Jun heterodimers interact with IRFs to stabilize binding of a heterocomplex to AICEs[25,26]. Both Batf and Batf3 can interact with both IRF4 and IRF8, but *Batf* is expressed neither in mature DCs nor in DC progenitors during development at homeostasis[25]. Like *Id2*, *Batf3* is expressed in both CD24^{+} and CD172a^{+} DCs, but is only required in development of CD24^{+} cDCs, both for splenic CD24^{+} and peripheral CD103^{+} cDCs that are the tissue-resident and migratory forms of the CD24^{+} DC lineage[7,27].

Batf3^{−/−} mice exhibit severe functional immune impairment[7,8,28]. However, there is an unexplained residual population of CD24^{+} cDCs in *Batf3*^{−/−} mice[25]. Therefore, it is possible that Batf3 may control gene expression only in mature CD24^{+} cDCs instead of controlling the development of this lineage, similar to the respective actions of EBF and Pax5 in B cell development[29]. If so, residual CD24^{+} cDCs in *Batf3*^{−/−} mice could represent cells undergoing abnormal development.

Here we present a model explaining the role of *Batf3* in CD24^{+} cDC development. First, we identify novel clonogenic progenitors that arise directly from the CDP which are committed to either CD24^{+} or CD172a^{+} cDCs. We show that the clonogenic progenitor of CD24^{+} cDCs, the pre-CD8 DC, can be specified without *Batf3*, but that *Batf3* is necessary at this stage to sustain *Irf8* autoactivation through an enhancer element that is exclusively active in CD24^{+} cDCs. In *Batf3*^{−/−} mice, this progenitor fails to commit to the CD24^{+} cDC lineage because of the decay of *Irf8* autoactivation and diverts into the IRF4^{+} CD172a^{+} lineage.

Results

IRF8 autoactivation occurs in early progenitors

We first confirmed the loss of CD24^{+} cDCs in *Irf8*^{−/−} mice[6] and BXH2 mice[17], which are homozygous for a mutation in IRF8 (R294C) that prevents IRF8 interaction with partner transcription factors PU.1, IRF2 and SpiB[17] (Fig. 1a). Unexpectedly, heterozygous *Irf8*^{+/−} mice had a 5-fold decrease in the frequency of CD24^{+} cDCs with decreased CD24 mean fluorescence intensity (MFI) (Fig. 1a), and similarly decreased CD8α^{+} CD205^{+} cells (Supplementary Fig. 1a). These decreases are greater than would be predicted from a 50%

reduction in IRF8 protein expression.[17,17] Similarly, there was 77% decrease in CD24^{+} cDC frequency in heterozygous $Irf8^{+/-}$ BM compared with wild-type BM and a 95% decrease in CD103^{+} cells using FLT3L-derived DCs (Fig. 1b). The heterozygous phenotype for CD24^{+} cDC development in $Irf8^{+/-}$ mice is consistent with IRF8 transcriptional autoactivation[30–32], in which IRF8 regulates its own transcription[19].

To find the developmental stage where $Irf8$ autoactivation occurs, we examined IRF8 protein expression in MDPs[33] and CDPs[13,14] (Fig. 1c, d). IRF8 expression was lower in wild-type MDPs as compared to CDPs, consistent with $Irf8$ reporter expression[34], and was only slightly decreased in $Irf8^{+/-}$ MDPs. IRF8 expression increased from wild-type MDPs to CDPs, but a smaller increase occurred in $Irf8^{+/-}$ CDPs. CDPs from BXH2 mice expressed less IRF8 than $Irf8^{+/-}$ CDPs (Fig. 1d, lower panel). These results suggest that $Irf8$ autoactivation occurs as early as the CDP stage and requires IRF8 interaction with a partner such as PU.1.

We expressed IRF8 by retrovirus in DC progenitors to test this hypothesis (Fig. 1e). Retroviral IRF8 increased development of CD24^{+} cDCs to 51% of total cDCs in $Irf8^{+/-}$ BM, compared with about 8% in the empty retrovirus control, whereas in $Irf8^{-/-}$ BM, CD24^{+} cDCs increased to only 14% of total cDCs (Fig. 1e). This suggests that efficient reconstitution by retroviral IRF8 requires an intact endogenous $Irf8$ locus. Moreover, expression of the IRF8 R294C protein increased CD24^{+} cDCs development only two fold in $Irf8^{+/-}$ but not at all in $Irf8^{-/-}$ BM (Fig. 1e), suggesting that the inability of IRF8 R294C protein to activate its own expression may in part cause the observed defect in CD24^{+} cDCs in BXH2 mice, similar to $Irf8^{-/-}$ mice[5,6].

We next examined whether retroviral IRF8 could induce endogenous IRF8 protein expression (Fig. 1f). FLT3L-treated wild-type BM cells infected with empty retrovirus had two distinct cDC populations with endogenous IRF8 expression that was either low (49%) or high (35%), while heterozygous $Irf8^{+/-}$ BM predominantly had cDCs with low endogenous IRF8 expression (64%) (Fig. 1f, left panels). Retroviral IRF8 achieved low IRF8 expression in 73% of infected $Irf8^{-/-}$ cDCs, but substantially increased the percentage of cells expressing high total IRF8 (retroviral and endogenous) in infected $Irf8^{+/-}$ (4.8% increased to 51%) and wild-type (35% increased to 73%) (Fig. 1f, right panels). Thus, the increase in total IRF8 protein induced by retroviral IRF8 in $Irf8^{+/-}$ cDCs compared to $Irf8^{-/-}$ cDCs occurred because of autoactivation at the endogenous $Irf8$ locus.

Analysis of IRF8 binding to the $Irf8$ locus by chromatin immunoprecipitation sequencing (ChIP-seq) showed several significant peaks of IRF8 binding located upstream and downstream of the $Irf8$ coding region but not at the $Irf8$ promoter (Fig. 1g). As a negative control, no peaks of IRF8 binding were observed in DCs derived from $Irf8^{-/-}$ BM. IRF8 binding to regulatory elements within the $Irf8$ locus is consistent with IRF8 autoactivation.

Batf3 maintains IRF8 in CD24^{+} cDCs

A direct interaction between the Batf3 leucine zipper and IRF8 is required for CD24^{+} cDC development[25]. Since IRF8 expression in CDPs involved an interaction between IRF8 and PU.1, we asked if IRF8 expression in mature CD24^{+} cDCs might also involve Batf3. $Irf8^{-/-}$

mice showed a compete loss of CD24$^+$ cDCs, but *Batf3*$^{-/-}$ mice retained a CD24$^+$ cDC population that was approximately 82% decreased compared with wild-type mice (Fig. 2a). Although certain infections can expand CD24$^+$ cDC frequency in *Batf3*$^{-/-}$ mice due to compensation by Batf2 or Batf[25], the persistence of these cells in uninfected *Batf3*$^{-/-}$ mice has never been explained.

Wild-type CD24$^+$ cDCs expressed high IRF8, however, the residual *Batf3*$^{-/-}$ CD24$^+$ cDCs had heterogeneous, decreased IRF8 expression (Fig. 2b). In contrast, pDCs expressed abundant IRF8 and CD172a$^+$ cDCs expressed much lower IRF8 in wild-type and *Batf3*$^{-/-}$ mice (Fig. 2b). Thus, residual CD24$^+$ cDCs in *Batf3*$^{-/-}$ mice are abnormal, expressing heterogeneous amounts of IRF8, suggesting a possible role for BATF3 in directly regulating IRF8 expression in this lineage.

cDC divergence occurs in bone marrow

CD24$^+$ and CD172a$^+$ cDCs share a common progenitor called the pre-conventional dendritic cell (pre-cDC), originally defined as lineage (Lin)$^-$ CD135$^+$ MHC II$^-$ CD11c$^+$ and developed from CDPs[35]. Since pre-cDCs had heterogeneous CD115 expression (Supplementary Fig. 1b.), we wondered if CD115 expression could distinguish pre-cDCs that were committed to either the CD24$^+$ or CD172a$^+$ cDC lineage. As a control, CDPs generated CD24$^+$ and CD172a$^+$ cDCs and pDCs, but the CD115$^+$ fraction of pre-cDCs developed exclusively into CD172a$^+$ cDCs (Supplementary Fig. 1c, d). In contrast, the CD115$^-$ fraction of pre-cDCs developed into both pDCs and CD172a$^+$ cDCs, consistent with a recent report showing that Lin$^-$ CD11c $^-$ CD135$^+$ CD115 $^-$ CD117^{int-lo} BM cells are enriched for pDC progenitors[36]. However, CD115$^-$ pre-cDCs did not develop into CD24$^+$ cDCs. Thus, surprisingly, neither fraction of the originally defined pre-cDC generated CD24$^+$ cDCs.

To identify the source of CD24$^+$ cDCs we used *Zbtb46*$^{GFP/+}$ mice, in which GFP expression identifies BM progenitors exclusively committed to cDC lineages and not pDCs[37]. Although pre-cDCs were originally defined as MHC II$^-$ cells[35], we noticed that strict exclusion of MHC II^{int} cells from the CD11c$^+$ pre-cDC gate identified cells that were CD117$^-$ and heterogeneous for *Zbtb46*-GFP expression (Fig. 3a, red gate). By including MHC II^{int} cells in the CD11c$^+$ pre-cDC gate, we identified an additional population of CD117^{int} *Zbtb46*-GFP$^+$ cells (Fig. 3a, blue gate), which were largely negative for CD115 (data not shown) (Fig 3a) and would have been excluded by the strict lineage gate used (Supplementary Fig. 1b). Therefore, we asked if these MHC II^{int} pre-cDCs might generate CD24$^+$ cDCs (Fig. 3). Indeed, these CD117^{int} *Zbtb46*-GFP$^+$ MHC II^{int} pre-cDCs developed exclusively into CD24$^+$ cDCs and lacked potential for both CD172a$^+$ cDCs and pDCs (Fig. 3b). By contrast, the CD115$^+$ CD117$^-$ MHC II$^-$ fraction of pre-cDCs developed exclusively into CD172a$^+$ cDCs (Fig. 3b and Supplementary Fig. 1c,d). Thus, commitment to distinct branches of cDCs can occur in the BM, and the definition of pre-cDCs can be refined. We will refer to these as pre-CD8 DCs (defined as Lin$^-$ CD135$^+$ CD11c$^+$ CD117^{int} MHC II^{int} *Zbtb46*-GFP$^+$ BM cells) and pre-CD4 DCs (defined as Lin$^-$ CD135$^+$ CD11c$^+$ CD117$^-$ CD115$^+$ BM cells) (Fig. 3b).

Pre-CD8 DCs arise directly from CDPs

To determine if pre-CD8 DCs develop directly from CDPs, we monitored FLT3L cultures of purified CDPs (Supplementary Fig. 2). CDPs rapidly acquired expression of CD11c, *Zbtb46*-GFP and MHC II, and diverged into two distinct populations distinguished by CD117 expression. One population retained intermediate CD117 expression, becoming CD117^{int} *Zbtb46*-GFP$^+$ CD11c$^+$ MHC II^{int} similar to pre-CD8 DCs (Supplementary Fig. 2b). The second population lost CD117 expression, resembling pre-CD4 DCs (CD117$^-$ *Zbtb46*-GFP$^+$ CD11c$^+$ MHC II$^-$). The pre-CD8 DC and pre-CD4 DCs have the morphology of immature progenitors similar to CDPs, with large nuclei, scant cytoplasm and lack of dendrites shown by mature cDCs (Fig. 3c). Previously, pre-cDCs were identifiable in both blood and spleen[35,38]. In agreement, a CD117^{int} MHC II^{int} *Zbtb46*-GFP$^+$ population resembling pre-CD8 DCs can be found in both blood and spleen (Fig. 3d).

We next examined the transcription factor requirements for specification of pre-CD8 DCs. *Zbtb46*-GFP$^+$ pre-CD8 DCs were present in BM at normal frequencies in *Batf3*$^{-/-}$ and *Irf4*$^{-/-}$ mice, but were absent in *Irf8*$^{-/-}$ mice (Fig. 4a). Previously, some splenic pre-cDCs that express CD24 were described as being largely committed to CD8α$^+$ cDCs[38]. We found that CD24 expression was restricted to the *Zbtb46*-GFP$^+$ CD117^{int} pre-CD8 DCs fraction (Fig. 4a,b). We tested whether CD24 expression could replace *Zbtb46*-GFP expression for identifying pre-CD8 DCs. Pre-CD8 cDCs identified by CD24 expression committed to CD24$^+$ cDCs exclusively and required *Irf8*, but not *Batf3* or *Irf4* to develop, similarly to those identified by *Zbtb46*-GFP (Fig. 4b, c). In summary, we have identified separate clonogenic progenitors for CD24$^+$ cDCs and CD172a$^+$ cDCs lineages that arise directly from CDPs. Pre-CD8 DCs developed in *Batf3*$^{-/-}$ mice but not in *Irf8*$^{-/-}$ mice and could be detected in blood and in spleen.

Novel cDC progenitors are developmentally discrete

We analyzed gene expression microarrays in BM CDPs, pre-CD8 DCs, and pre-CD4 DCs and splenic CD24$^+$ and CD172a$^+$ cDCs (Fig. 5). By principal component analysis (PCA), all progenitors segregated from mature cDC subsets along principal component (PC) 1, accounting for approximately half of all variation (Fig. 5a). Pre-CD8 DCs and CD24$^+$ cDCs clustered together and segregated from pre-CD4 DCs and CD172$^+$ cDCs (Fig. 5a, b) along PC2 and PC3, accounting for nearly all remaining variation. In pairwise comparisons (Fig. 5c–d), expression of some genes changed at different stages during CD24$^+$ cDC development and CD172a$^+$ cDC development, including some genes that are equally expressed in both mature cDC subsets. For example, *H2-Aa*, encoding an isotype of MHC class II, was fully induced during the transition from CDP to pre-CD8 DC but induced only to an intermediate amount in pre-CD4 DCs. In contrast, myeloperoxidase (*Mpo*) and cathepsin G (*Ctsg*) were fully downregulated during the CDP to pre-CD4 DC transition, but decreased to an intermediate level in pre-CD8 DCs. Hierarchical clustering further showed that pre-CD8 and pre-CD4 DCs are distinct from CDPs and each other (Fig. 5e) as well as from mature cDC subsets (Fig. 5f).

Many transcription factor genes showed stage-specific regulation (Fig. 5g). For example, *Batf3* and *Id2* were upregulated during the CDP to pre-CD8 DC transition to the level in

mature CD24$^+$ cDCs, but their upregulation was delayed during CD172a$^+$ cDC development. (Fig. 5h). In contrast, *Nr4a1* (*Nur77*), *Nr4a2*, and *Nr4a3* were upregulated only during the transition from pre-CD8 to mature CD24$^+$ cDC. Interestingly, *Irf8* is still expressed in pre-CD4 DCs and is not downregulated until the mature CD172a$^+$ cDC stage. In contrast, *Irf4* is not highly expressed in pre-CD4 DCs, but rather only in mature CD172a$^+$ cDCs (Fig. 5h, i). Because *Zbtb46*$^{GFP/+}$ cells were used to identify pre-CD8 and pre-CD4 DCs, *Zbtb46* transcript increased modestly during CDP to pre-CD8 and pre-CD4 DC transitions. Taken together, these data suggest that pre-CD4 DCs and pre-CD8 DCs represent discrete stages of development.

A *Batf3*-dependent enhancer controls *Irf8* expression

We sought evidence for a direct role of Batf3 in regulating *Irf8* expression. Thus, we performed chromatin immunoprecipitation sequencing (ChIP-seq) for IRF8 in CD24$^+$ cDCs and pDCs where it is strongly expressed, and Batf3 in CD24$^+$ cDCs and CD172a$^+$ cDCs where it is expressed (Supplementary Fig. 3a, b, Fig. 6a). In CD24$^+$ cDCs, Batf3 and IRF8 binding were co-localized at sites −26 kilobases (kb) and +32 kb from the *Irf8* transcriptional start site (TSS) (Fig. 6a). IRF8, but not Batf3, also bound at sites −16 kb and +41 kb from the *Irf8* TSS in both CD24$^+$ cDCs and pDCs. In CD24$^+$ cDCs and pDCs, binding of the histone acetyltransferase p300, indicating enhancer activity, was observed at both the +32 kb and +41 kb elements (Fig. 6a). In CD172a$^+$ cDCs, which express Irf4, the *Irf8* locus lacked p300 and Batf3 binding, suggesting that the Batf3-IRF8 heterodimers rather than Batf3-IRF4 heterodimers may bind preferentially.

Recently, superenhancers have been recognized as critical in controlling cell identity[39,40]. The *Irf8* locus showed high ChIP signals for acetylation of histone H3 lysine 27 (H3K27ac) and monomethylation of histone H3 lysine 4 (H3K4me1) throughout a 60 kb region in CD24$^+$ cDCs and pDCs, and had H3K4me1 binding but no H3K27Ac binding in CD172a$^+$ cDCs (Fig. 6a). Thus, the *Irf8* locus is poised but not active in CD172a$^+$ cDCs. H3K4me1 and H2K27ac binding were depleted at the locations of the +32 kb and +41 kb *Irf8* peaks in CD24$^+$ cDCs (Supplementary Fig. 3c). The *Irf8* locus was the top-ranked superenhancer region using normalized H3K27ac ChIP-seq signal in CD24$^+$ cDC and pDCs, but did not rank as a superenhancer in CD172a$^+$ cDCs (Supplementary Fig. 4a–c). Superenhancers with distinct DC specificity could be identified (Supplementary Fig. 4d). For example, a superenhancer at the *Itgae* locus was specific for CD24$^+$ cDCs and a superenhancer for the *Bcl11a* locus was specific for pDCs. The *Id2* locus had superenhancer activity in both CD24$^+$ and CD172a$^+$ cDCs. In summary, the +32 kb region in *Irf8* binds Batf3, IRF8 and p300 and is contained within an *Irf8* superenhancer.

The activity of several of these genomic regions was tested using retroviral reporters in FLT3L-derived DCs[41–43] (Fig. 6b, Supplementary Fig. 5a–d). The *Irf8* minimal promoter, either alone or *in cis* with the −26 kb *Irf8* region, was inactive in all DC subsets. The −16 kb element and a previously identified PU.1-binding element at −50 kb[44] were generally active in all DC subsets, remained active in *Batf3*$^{−/−}$ pDCs and had slightly increased activity in *Batf3*$^{−/−}$ CD172a$^+$ cDCs, perhaps reflecting an original commitment of some of these cells to the CD24$^+$ lineage (Supplementary Fig. 5b, c). In contrast, the +32 kb element was active

specifically in CD24^{+} cDCs but not in CD172a^{+} cDCs or pDCs, and its activity was decreased in the few remaining *Batf3*^{−/−} CD24^{+} cDCs (Fig. 6b, Supplementary Fig. 5a–c). Conversely, the +41 kb element was active specifically in pDCs and not CD24^{+} DCs, and remained active in *Batf3*^{−/−} pDCs. *De novo* motif discovery showed that the AICE motif was enriched within Batf3 binding peaks in CD24^{+} cDCs (Supplementary Fig. 6a) and was contained four times within the +32 kb element[25,26] (Supplementary Fig. 6b–e). AICE sites 1 and 2 are the most highly conserved between mouse and human (Supplementary Fig. 6d,e). Thus, Batf3-dependent *Irf8* autoactivation in CD24^{+} cDCs may operate at an element at +32 kb within an Irf8 superenhancer.

IRF8 expression becomes dependent on Batf3

Next we asked which stage of CD24^{+} cDC development requires Batf3 (Fig. 7). In the BM, pre-CD8 DCs appear at similar frequencies in *Batf3*^{−/−} and wild-type mice (Fig. 7a) but are decreased by about 40% in blood and spleen of *Batf3*^{−/−} compared to wild-type mice (Fig. 7a, b). The amount of IRF8 protein was similar in *Batf3*^{−/−} mice and wild-type BM pre-CD8 DCs. However, *Batf3*^{−/−} pre-CD8 DCs in blood and spleen had lower levels of IRF8 than that of their wild-type counterparts (Fig. 7c,d).

To determine the eventual fate of pre-CD8 DCs in *Batf3*^{−/−} mice, we monitored the differentiation of CDPs, pre-CD8 DCs, and pre-CD4 DCs from wild-type and *Batf3*^{−/−} mice over 5 days of FLT3L culture (Fig. 7e,f). As expected, wild-type CDPs produced both CD24^{+} and CD172a^{+} cDCs, and pre-CD4 DCs from wild-type and *Batf3*^{−/−} mice produced exclusively CD172a^{+} DCs. Wild-type and *Batf3*^{−/−} pre-CD8 DCs initially expressed CD24 in the BM (Fig. 4b), but *Batf3*^{−/−} pre-CD8 DCs progressively downregulated CD24 and gained CD172a (Fig. 7e,f). *Batf3*^{−/−} pre-CD8 DCs initially expressed abundant IRF8, but IRF8 was rapidly decreased to the amount expressed by wild-type CD172a^{+} DCs (Fig. 7g, h).

Similarly, wild-type pre-CD4 DCs in BM were heterogeneous for IRF8 expression, with 38% exhibiting high IRF8 protein expression (Supplementary Fig. 7a), in agreement with high *Irf8* transcription in pre-CD4 DCs (Fig. 5h). However, IRF8 expression was lost by day 1 during FLT3L culture of pre-CD4 DCs (Supplementary Fig. 7b). The low *Batf3* expression by pre-CD4 DCs (Fig. 5h) and the instability of IRF8 expression in pre-CD4 DCs were consistent with a requirement for Batf3 in maintaining IRF8 expression in cDCs. In summary, these results suggest that pre-CD8 DCs are specified normally in *Batf3*[−\ −] mice, but convert to the CD172a^{+} cDC lineage because they fail to maintain IRF8 expression.

Transgenic IRF8 overexpression bypasses Batf3 dependence

The murine *Irf8*[VENUS] reporter carries three copies of a phage artificial chromosome (PAC) containing a 130 kb *Irf8* genomic region harboring an *ires*-VENUS cassette within the *Irf8* 3′-UTR[44] resulting in five *Irf8* loci each containing all of the recognized regulatory elements. VENUS expression reproduced the expected IRF8 expression in mature wild-type DC subsets[44] but has not been examined in *Batf3*^{−/−} mice. Wild-type *Irf8*[VENUS+/−] mice developed splenic DC subsets normally (Fig. 8a), albeit with slightly increased CD24 MFI in CD24^{+} cDCs, with high VENUS expression in CD24^{+} cDCs and pDCs and low

expression in CD172a$^+$ cDCs (Supplementary Fig. 8). Thus, development of wild-type CD24$^+$ cDCs is not affected by increased IRF8. Surprisingly, *Batf3$^{-/-}$ Irf8$^{\mathrm{VENUS+/-}}$* mice showed restored splenic CD24$^+$ cDC development compared to *Batf3$^{-/-}$* mice (Fig. 8a). Residual CD24$^+$ cDCs in *Batf3$^{-/-}$* mice had decreased IRF8 expression, as before; however, CD24$^+$ cDCs in *Batf3$^{-/-}$ Irf8$^{\mathrm{VENUS+/-}}$* mice maintained IRF8 (Fig. 8b,c). These results show that increased IRF8 protein expression in *Batf3$^{-/-}$ Irf8$^{\mathrm{VENUS}}$* mice bypasses the requirement for Batf3 in *Irf8* autoactivation.

These actions of *Irf8$^{\mathrm{VENUS}}$* on pre-CD8 DCs were apparent in BM as well (Fig. 8d–f). BM MHC II$^{\mathrm{int}}$ pre-CD8 DCs matured normally into MHC II$^{\mathrm{hi}}$ IRF8$^+$ cDCs (Fig. 8d). In contrast, *Batf3$^{-/-}$* pre-CD8 DCs lost IRF8 as they matured and acquired MHC II (Fig. 8d, lower right panel). However, this loss of IRF8 was reversed in *Batf3$^{-/-}$ Irf8$^{\mathrm{VENUS+/-}}$* mice (Fig. 8e, f). In summary, the normal requirement for Batf3 in *Irf8* autoactivation can be bypassed by increasing the number of copies of endogenous *Irf8* loci.

Discussion

This study extends our understanding of DC development by identifying committed clonogenic precursors of CD24$^+$ and CD172a$^+$ cDCs, which represent the CD8α$^+$ and CD4$^+$ cDC lineages, respectively. These findings were made possible by the use of *Zbtb46$^{\mathrm{GFP}}$* reporter mice in which *Zbtb46*-GFP$^+$ BM progenitors are committed to cDC fates and exclude pDC potential[37]. Previously, pre-cDCs were not defined on the basis of CD117 expression[35], but contained both CD117$^{\mathrm{int}}$ and CD117$^{\mathrm{neg}}$ cells. We show that CD117 expression among *Zbtb46*-GFP$^+$ pre-cDCs can distinguish clonogenic CD8α$^+$ and CD4 cDC progenitors that are CD117$^{\mathrm{int}}$ and CD117$^-$ respectively. The CD117$^-$ fraction of pre-cDCs excluded CD24$^+$ DC potential, however, it was heterogeneous for CD115 (MCSF-R) expression. While CD117$^-$ CD115$^+$ pre-cDCs were mostly *Zbtb46*-GFP$^+$ and developed exclusively into CD172a$^+$ cDCs, CD117 $^-$ CD115$^-$ pre-cDCs were mostly *Zbtb46*-GFP$^-$ and retained potential for both pDCs and CD172a$^+$ cDCs, consistent with a report indicating a bias of CD115$^-$ progenitors for the pDC fate[36]. An exclusive pDC progenitor has not been defined[45].

Transcriptional autoactivation circuits can stabilize lineage fate decisions [30]. As an example, we have shown that GATA-3 autoactivation stabilizes T$_H$2 development[31]. *Irf8* autoactivation has been suggested previously[19,34], but had not been examined during DC development. A recent study showed that a PU.1-dependent enhancer at −50 kb in the *Irf8* locus initially drives *Irf8* expression in MDPs[44]. We show that the increase in IRF8 expression in CDPs is sensitive to the IRF8 R294C mutation which influences IRF8 interaction with PU.1 as well as IRF2 and SpiB [17,46,47]. This extends the role of PU.1 to also include *Irf8* autoactivation in early BM progenitors.

We show that commitment, but not specification, to the CD24$^+$ cDC lineage is Batf3-dependent. Batf3 is induced during specification in wild-type pre-CD8 DCs along with Id2 and is required to sustain *Irf8* autoactivation. Without Batf3, IRF8 decays in the progeny of pre-CD8 DCs, which then do not commit to the CD24$^+$ cDC lineage but divert towards

CD172a^{+} cDCs. Further studies are required to determine the transcription factors involved in specification of pre-CD8 and pre-CD4 DCs.

The normal loss of IRF8 in the CD172a^{+} DC lineage can also be explained as a lack of Batf3-dependent *Irf8* autoactivation. Pre-CD4 DCs express IRF8 heterogeneously but do not yet express *Batf3*. This indicates that commitment to CD172a^{+} cDCs occurs before complete loss of IRF8 and suggests that *Irf8* transcription decays at this stage, as in *Batf3*^{−/−} pre-CD8 DCs, because of the lack of Batf3. Thus, the delay of *Batf3*, and possibly *Id2*, in pre-CD4 DCs relative to pre-CD8 DCs may explain differential IRF8 expression between the lineages. Conceivably, the E3 ligase Cbl, which can promote IRF8 protein degradation[48], could regulate differential IRF8 expression: however since *Cbl* is uniformly expressed across all stages, this seems unlikely. Competition with IRF4 is also a possible mechanism. However IRF4 is not abundantly expressed in pre-CD4 cDCs.

Importantly, while CD24^{+} cDCs require Batf3 for sustained *Irf8* expression, pDCs do not. The *Irf8* locus has the characteristics of a superenhancer in both CD24^{+} cDCs and pDCs[39,40], but uses different enhancer elements in those two lineages. An element located at +32 kb relative to the *Irf8* TSS binds IRF8, Batf3 and p300, and has enhancer exclusively in CD24^{+} cDCs, while an element located at +41 kb binds IRF8 and p300, but not Batf3, and functions in pDCs.

Batf and Batf2 can compensate for Batf3 in CD24^{+} cDC development during infections[25]. However, this does not explain residual CD8α^{+} CD103^{+} cDCs observed in uninfected *Batf3*^{−/−} mice[7] which nonetheless are impaired in several pathogen models *in vivo*[7,8,28,49]. Here, we find that residual CD24^{+} cDCs in *Batf3*^{−/−} mice express heterogeneous IRF8 undergoing transcriptional decay and are likely non-functional. IRF8 maintenance in *Batf3*^{−/−} mice rescues splenic CD24^{+} cDC development, but whether all the functions of cells are restored, or depend on Batf3, will require further study.

Online Methods

Mice

Zbtb46[GFP/+] mice were neomycin cassette-deleted, N8 and N9 backcrosses from 129S6/SvEvTac to C57BL/6J. *Batf3*^{−/−} and *Irf8*[VENUS] have been described[7,44]. *Irf8*^{−/−} mice were generated by crossing *Irf8*[f/f] mice (B6(Cg)-*Irf8*[tm1.1Hm]/J, Jackson Laboratories) with CMV-Cre mice (B6.C-Tg(CMV-cre)1Cgn/J). *Irf8*^{+/−} mice were obtained by crossing *Irf8*^{−/−} mice to wild-type C57BL/6J.

Irf4^{−/−} mice were generated by crossing *Irf4*[f/f] mice (B6.129S1-*Irf4*[tm1Rdf]/J, Jackson Laboratories) first to CMV-Cre mice (B6.C-Tg(CMV-cre)1Cgn/J) and then to CMV-Flp1 mice (B6.129S4-*Gt(ROSA)26Sor*[tm1(FLP1)Dym]/JRainJ). BXH2/TyJ mice were from The Jackson Laboratory. All mice were maintained on the C57BL/6J background and maintained in a specific pathogen-free animal facility following institutional guidelines and with protocols approved by the Animal Studies Committee at Washington University in St. Louis. Experiments were performed with mice 8–12 weeks of age using sex-matched littermates.

Antibodies and flow cytometry

Cells were kept at 4°C while staining in PBS with 0.5% BSA and 2 mM EDTA in the presence of CD16/32 block (BD clone 2.4G2).

The following antibodies were purchased from BD: CD45.1 BV711 (A20), CD117 BUV395 (2B8), CD135 APC & PE-CF594 (A2F10.1), MHC II V500, BV421, BV510 (M5/114.15.2), CD24 BUV496 (M1/69), CD127 BV421 (SB/199), CD45RA PE (14.8), CD19 BV42 1(1D3). From eBioscience: CD117 PE-Cy7 (2B8), CD317 eFluor450 & APC (eBio927), CD115 PE (AFS98), APC eFluor780 anti-CD11c (N418), MHC II eFluor450 (M5/114/15/2), CD24 PE-Cy7 (M1/69), CD172a APC & PerCP-eFluor710 (P84), Siglec-H PerCP-eFluor710 (eBio440C), eFluor450 Ter119 (Ter119), CD105 eFluor450 (MJ7/18), Irf8 PerCP-eFluor710 (V3GYWCH), CD45R eFluor450 (RA3-6B2), NK1.1 eFluor450 (PK136), CD3 eFluor450 (17A2), Irf4 PE (3E4). From Tonbo Biosciences: CD45.1 PE-Cy7 (A20), CD115 PE (AFS98), CD11c APC-Cy7 (N418). From BioLegend: CD115 BV711 (ASF98), CD45.1 Alexa Fluor 488 (A20), Flag (DYKDDDDK) APC (L5).

Lineage cell depletion kit was purchased from Miltenyi. Cells were analyzed on FACSCanto II or FACSAria Fusion flow cytometers (BD), and data analyzed with FlowJo software (Tree Star).

Isolation and culture of BM progenitor cells and splenic DCs

BM was harvested from pelvis, tibia, and femurs using mortar and pestle in PBS supplemented with 0.5% BSA and 2 mM EDTA, passed through a 70-μm strainer, and red blood cells lysed with ACK lysis buffer. For some experiments, BM was purified on Histopaque-119 (Sigma-Aldrich) gradient prior to culture or sorting. Gates used to define the MDP, CDP, and pre-cDC are based on previous studies[13,35]. BM was treated using lineage depletion beads (Miltenyi) before sorting. MDPs were identified as Lin− CD117^{hi} CD135+ CD115+ BM cells; CDPs as Lin− CD117^{int} CD135+ CD115+ CD11c− MHC II− BM cells; pre-CD8 DCs as Lin− CD135+ CD117^{int} Siglec H− CD11c+ MHC II^{int} BM cells; and pre-CD4 DCs as Lin− CD135+ CD117^{low} CD115+ CD11c+ MHC II− BM cells. Lin includes CD19, B220, CD3, NK1.1, CD105, and TER-119, or as indicated in the figure legend. Blood and spleen pre-cDCs were sorted as Lin− MHC II$^{int-neg}$ CD172$^{int-neg}$ CD11c+ CD135+. Lin for blood and spleen includes CD19, B220, CD3, NK1.1, TER-119. FACSAria Fusion was used for sorting cells in into IMDM + 10% FCS (cIMDM) with 100 ng/ml Flt3L. For DC preparation, spleens were minced and stirred at 37°C in 5 ml of cIMDM with 30 U/ml DNase I (Sigma-Aldrich) and 250 μg/ml collagenase B (Roche) for 30 min. To remove debris, cells were passed through a 70-μm strainer before red blood cells were lysed with ACK lysis buffer. For Flt3L culture experiments[50], sorted cells ($3–6 \times 10^3$ cells/200 μl cIMDM) were cultured at 37°C in 100 ng/ml Flt3L (PeproTech) for 1–5 days.

Expression microarray analysis

RNA extraction was performed using the RNAqueous-Micro Kit (Ambion), amplified using the Ovation Pico WTA Sytem (NuGEN), and hybridized to GeneChip Mouse Gene 2.0 ST microarrays (Affymetrix). Fragmentation was performed with the NuGen Encore biotin module and samples were hybridized in a GeneChip Hybridization Oven 640 for 18 h at 45

°C. Data normalization was performed using robust multiarray average (RMA) summarization and quartile normalization using ArrayStar software (DNASTAR). CDP and CD24^{+} cDC expression values were averaged from biological triplicates, and all other expression values were averaged from biological duplicates. Principal component analysis was computed by singular value decomposition without additional centering or scaling after samples were grouped by replicate and the mean log-transformed expression values from each group imported into R, mean-centered by gene, root mean square (RMS)-scaled by sample, and transposed. Unsupervised hierarchical clustering of differentially expressed genes was computed using ArrayStar (DNAstar) with a Euclidean distance metric and centroid linkage method.

Retroviral analysis

Retroviral vectors were transfected into Phoenix-E cells as described previously[25] and viral supernatants were collected 2 d later. BM cells were infected with supernatants of transfected packaging cells, concentrated by centrifugation [51] with 2 μg/ml polybrene using spin infection at 1800 rpm for 45 min. Infected cells were cultured in Flt3L as previously described[25].

Genomic enhancer elements were cloned into a retroviral reporter (hCD4 pA GFP RV) [41–43] using primers shown in Supplementary Table 1. For analysis, we used integrated MFI, which combines the metrics of frequency and MFI as a measure of total functional response[52,53].

Generation of Batf3-specific rabbit polyclonal antibody

Murine *Batf3* cDNA was generated by RT-PCR from CD8α[+] cDCs, cloned into pET-28a(+) (Novagen) downstream of the His tag, and protein generated in *E. coli* BL21-CodonPlus(DE3)-RIL (Stratagene). Recombinant Batf3 was expressed for 12 h at 22 °C, purified on Ni-NTA His·Bind Resin (Novagen), and used to immunize New Zealand White Rabbits (Harlan Laboratories). Anti-Batf3 antibody was affinity purified[54].

Chromatin immunoprecipitation

ChIP was performed as described[54] with minor modifications. CD24^{+} and CD172a^{+} cDCs and pDCs from FLT3L-treated BM cultures of wild-type mice were sort-purified on day 9. For p300 ChIP, sorted cells were incubated in fresh media with FLT3L for 2 hours before crosslinking. For IRF8, Batf3, H3K27ac, and H3K4me1ChIP, cells were crosslinked before sorting. Cells were crosslinked with 1% formaldehyde for 10 min at 37°C for p300 ChIP or for 8 min at room temperature for IRF8, Batf3, H3K27ac and H3K4me1 ChIP, quenched with 1.25M glycine, washed twice with PBS and pellets were flash frozen for storage at −80 °C. Chromatin was sonicated at 4°C in sonication buffer (10 mM Tris-HCl pH8, 100 mM NaCl, 1 mM EDTA, 0.5 mM EGTA, 0.1% sodium deoxycholate, 0.5% N-lauroylsarcosine) for 36 cycle (p300), or 22 cycle (IRF8, Batf3, H3K27ac, and H3K4me1) of 20 s on and 50 s off per cycle using Vivra-Cell VCX130PB and CV188 (SONICS & MATERIAL.INC) to obtain DNA fragments from 140 to 500 bp. Chromatin was immunoprecipitated overnight at 4 °C with Dynabeads Protein A or G (Invitrogen) that had been pre-incubated with 1–6 μg of the appropriate antibody: anti-p300 (sc-585X, Santa Cruz Biotechnology), anti-IRF8

(sc-6058x, Santa Cruz Biotechnology), anti-Batf3, anti-H3K27ac (Ab 4729, Abcam) or H3K4me1 (Ab 8895, Abcam). Beads containing protein-DNA complexes were washed with RIPA buffer 7 times and Tris-EDTA + 50mM NaCl. DNA fragments were eluted and crosslinking was reversed by incubation at 65 °C for 6 h in 50 mM Tris-HCl, pH 8.0, 10 mM EDTA and 1% SDS with 1mg/ml Proteinase K (New England Biolabs). DNA was purified with phenol:chloroform extraction followed by ethanol precipitation. Libraries for ChIP-seq were prepared using ThruPLEX-FD kit (Rubicon Genomics) and sequenced using Illumina HiSeq 2500 as single reads extending 50 bases.

Computational analysis

ChIP-Seq data sets were aligned to the mouse genome (NCBI37/mm9) by Bowtie[55] version 1.0.1 with the following parameters: --sam --best -p 4 -m 1 mm9 --chunkmbs 4000. Uniquely mapped reads were masked using samtools[56] with blacklist of ENCODE Project[57] and RepeatMasker (http://www.repeatmasker.org) in the UCSC Genome Browser. Reads for BATF3 and IRF8 ranged from 6274983 to 9234602, for p300 9745561 to 11293164, for H3K4me1 6599991 to 8402016 and for H3K27ac 8065509 to 11950695. Data were visualized using the 'makeUCSCfile' program of the Homer software package with default parameters[58].

Peaks were identified using (Model-based Analysis for ChIP-Seq)[59] MACS version 1.4.2 with p-value 1e-9. For motif analysis, we selected the top 1,000 peaks with lowest *P* values, extracted 150 bp centered on the summit for each peak, and performed motif analysis using MEME software[60]. AICE motif occurrence in the +32 kb element was found using FIMO[60] at a P-value threshold of 1e-3 with the AICE position weight matrix obtained from CD24+DC Batf3 peaks.

Superenhancer analysis

Superenhancers were identified as described[39,61] using ROSE (Rank Ordering of Superenhancers) with flag -t 2500 with a stitching distance of 12,500 bp and a promoter exclusion zone of TSS ± 2,500 bp. ROSE ranked all enhancers by increasing total background-subtracted ChIP-seq occupancy of H3K27ac, and plotted the total background-subtracted ChIP-seq occupancy of H3K27ac. Superenhancers were identified by an inflection point of H3K27ac signal versus enhancer rank[61]. Superenhancers were assigned to the genes whose TSS site was the nearest from the center of the superenhancer and which had an H3K27ac peak within TSS ± 1kb.

Statistical analysis

Statistical analyses were performed using Prism (GraphPad Software) as indicated in the figure legends. All *t*-tests were performed on samples that passed a normality test and showed no statistical difference in their variance. Unpaired *t*-tests on samples that had unequal variances, as shown by an *F*-test, were performed with Welch's correction. All one-way ANOVA were performed on samples that passed a normality test and showed no statistical difference in their standard deviation as shown by a Brown-Forsythe test. Samples that could not be tested for normality were analyzed with a Mann-Whitney *U* test.

Supplementary Material

Refer to Web version on PubMed Central for supplementary material.

Acknowledgments

Reference List

1. Satpathy AT, et al. Re(de)fining the dendritic cell lineage. Nat Immunol. 2012; 13:1145–1154. [PubMed: 23160217]

2. Cervantes-Barragan L, et al. Plasmacytoid dendritic cells control T-cell response to chronic viral infection. Proc Natl Acad Sci U S A. 2012; 109:3012–3017. [PubMed: 22315415]

3. Reizis B, et al. Plasmacytoid dendritic cells: recent progress and open questions. Annu Rev Immunol. 2011; 29:163–183. [PubMed: 21219184]

4. Vremec D, et al. CD4 and CD8 expression by dendritic cell subtypes in mouse thymus and spleen. Journal of Immunology. 2000; 164:2978–2986.

5. Aliberti J, et al. Essential role for ICSBP in the in vivo development of murine CD8alpha + dendritic cells. Blood. 2003; 101:305–310. [PubMed: 12393690]

6. Tamura T, et al. IFN regulatory factor-4 and -8 govern dendritic cell subset development and their functional diversity. The Journal of Immunology. 2005; 174:2573–2581. [PubMed: 15728463]

7. Hildner K, et al. Batf3 deficiency reveals a critical role for CD8alpha+ dendritic cells in cytotoxic T cell immunity. Science. 2008; 322:1097–1100. [PubMed: 19008445]

8. Torti N, et al. Batf3 transcription factor-dependent DC subsets in murine CMV infection: differential impact on T-cell priming and memory inflation. European Journal of Immunology. 2011; 41:2612–2618. [PubMed: 21604258]

9. Persson EK, et al. IRF4 Transcription-Factor-Dependent CD103(+)CD11b(+) Dendritic Cells Drive Mucosal T Helper 17 Cell Differentiation. Immunity. 2013; 38:958–969. [PubMed: 23664832]

10. Gao Y, et al. Control of T helper 2 responses by transcription factor IRF4-dependent dendritic cells. Immunity. 2013; 39:722–732. [PubMed: 24076050]

11. Schlitzer A, et al. IRF4 Transcription Factor-Dependent CD11b(+) Dendritic Cells in Human and Mouse Control Mucosal IL-17 Cytokine Responses. Immunity. 2013; 38:970–983. [PubMed: 23706669]

12. Merad M, Ginhoux F. Dendritic cell genealogy: a new stem or just another branch? Nat Immunol. 2007; 8:1199–1201. [PubMed: 17952047]

13. Onai N, et al. Identification of clonogenic common Flt3(+) M-CSFR+ plasmacytoid and conventional dendritic cell progenitors in mouse bone marrow. Nature Immunology. 2007; 8:1207–1216. [PubMed: 17922016]

14. Naik SH, et al. Development of plasmacytoid and conventional dendritic cell subtypes from single precursor cells derived in vitro and in vivo. Nat Immunol. 2007; 8:1217–1226. [PubMed: 17922015]

15. Schiavoni G, et al. ICSBP is essential for the development of mouse type I interferon-producing cells and for the generation and activation of CD8alpha(+) dendritic cells. J Exp Med. 2002; 196:1415–1425. [PubMed: 12461077]

16. Suzuki S, et al. Critical roles of interferon regulatory factor 4 in CD11bhighCD8alpha- dendritic cell development. Proc Natl Acad Sci US A. 2004; 101:8981–8986.

17. Tailor P, et al. The BXH2 mutation in IRF8 differentially impairs dendritic cell subset development in the mouse. Blood. 2008; 111:1942–1945. [PubMed: 18055870]

18. Kantakamalakul W, et al. Regulation of IFN consensus sequence binding protein expression in murine macrophages. Journal of Immunology. 1999; 162:7417–7425.

19. Bornstein C, et al. A negative feedback loop of transcription factors specifies alternative dendritic cell chromatin States. Mol Cell. 2014; 56:749–762. [PubMed: 25453760]

20. Vander, Lugt B., et al. Transcriptional programming of dendritic cells for enhanced MHC class II antigen presentation. Nat Immunol. 2014; 15:161–167. [PubMed: 24362890]

21. Hacker C, et al. Transcriptional profiling identifies Id2 function in dendritic cell development. Nat Immunol. 2003; 4:380–386. [PubMed: 12598895]

22. Spits H, et al. Id2 and Id3 inhibit development of CD34(+) stem cells into predendritic cell (pre-DC)2 but not into pre-DC1. Evidence for a lymphoid origin of pre-DC2. J Exp Med. 2000; 192:1775–1784. [PubMed: 11120774]

23. Li HS, et al. The signal transducers STAT5 and STAT3 control expression of Id2 and E2-2 during dendritic cell development. Blood. 2012; 120:4363–4373. [PubMed: 23033267]

24. Ghosh HS, et al. ETO family protein Mtg16 regulates the balance of dendritic cell subsets by repressing Id2. Journal of Experimental Medicine. 2014; 211:1623–1635. [PubMed: 24980046]

25. Tussiwand R, et al. Compensatory dendritic cell development mediated by BATF-IRF interactions. Nature. 2012; 490:502–507. [PubMed: 22992524]

26. Glasmacher E, et al. A Genomic Regulatory Element That Directs Assembly and Function of Immune-Specific AP-1-IRF Complexes. Science. 2012; 338:975–980. [PubMed: 22983707]

27. Edelson BT, et al. Peripheral CD103+ dendritic cells form a unified subset developmentally related to CD8alpha+ conventional dendritic cells. Journal of Experimental Medicine. 2010; 207:823–836. [PubMed: 20351058]

28. Mashayekhi M, et al. CD8a+ Dendritic Cells Are the Critical Source of Interleukin-12 that Controls Acute Infection by Toxoplasma gondii Tachyzoites. Immunity. 2011; 35:249–259. [PubMed: 21867928]

29. Medvedovic J, et al. Pax5: a master regulator of B cell development and leukemogenesis. Adv Immunol. 2011; 111:179–206. [PubMed: 21970955]

30. Veraksa A, Del Campo M, McGinnis W. Developmental patterning genes and their conserved functions: from model organisms to humans. Mol Genet Metab. 2000; 69:85–100. [PubMed: 10720435]

31. Ouyang W, et al. Stat6-independent GATA-3 autoactivation directs IL-4-independent Th2 development and commitment. Immunity. 2000; 12:27–37. [PubMed: 10661403]

32. Boyer LA, et al. Core transcriptional regulatory circuitry in human embryonic stem cells. Cell. 2005; 122:947–956. [PubMed: 16153702]

33. Fogg DK, et al. A clonogenic bone marrow progenitor specific for macrophages and dendritic cells. Science. 2006; 311:83–87. [PubMed: 16322423]

34. Wang H, et al. A reporter mouse reveals lineage-specific and heterogeneous expression of IRF8 during lymphoid and myeloid cell differentiation. Journal of Immunology. 2014; 193:1766–1777.

35. Liu K, et al. In vivo analysis of dendritic cell development and homeostasis. Science. 2009; 324:392–397. [PubMed: 19286519]

36. Onai N, et al. A clonogenic progenitor with prominent plasmacytoid dendritic cell developmental potential. Immunity. 2013; 38:943–957. [PubMed: 23623382]

37. Satpathy AT, et al. Zbtb46 expression distinguishes classical dendritic cells and their committed progenitors from other immune lineages. Journal of Experimental Medicine. 2012; 209:1135–1152. [PubMed: 22615127]

38. Naik SH, et al. Intrasplenic steady-state dendritic cell precursors that are distinct from monocytes. Nat Immunol. 2006; 7:663–671. [PubMed: 16680143]

39. Whyte WA, et al. Master transcription factors and mediator establish super-enhancers at key cell identity genes. Cell. 2013; 153:307–319. [PubMed: 23582322]

40. Hnisz D, et al. Super-enhancers in the control of cell identity and disease. Cell. 2013; 155:934–947. [PubMed: 24119843]

41. Zhu H, et al. Unexpected characteristics of the IFN-gamma reporters in nontransformed T cells. Journal of Immunology. 2001; 167:855–865.

42. Schraml BU, et al. The AP-1 transcription factor Batf controls T(H)17 differentiation. Nature. 2009; 460:405–409. [PubMed: 19578362]

43. Ise W, et al. The transcription factor BATF controls the global regulators of class-switch recombination in both B cells and T cells. Nat Immunol. 2011; 12:536–543. [PubMed: 21572431]

44. Schonheit J, et al. PU.1 level-directed chromatin structure remodeling at the Irf8 gene drives dendritic cell commitment. Cell Rep. 2013; 3:1617–1628. [PubMed: 23623495]

45. Reizis B, et al. Plasmacytoid dendritic cells: one-trick ponies or workhorses of the immune system? Nat Rev Immunol. 2011; 11:558–565. [PubMed: 21779033]

46. Ichikawa E, et al. Defective development of splenic and epidermal CD4+ dendritic cells in mice deficient for IFN regulatory factor-2. Proc Natl Acad Sci US A. 2004; 101:3909–3914.

47. Nagasawa M, et al. Development of human plasmacytoid dendritic cells depends on the combined action of the basic helix-loop-helix factor E2-2 and the Ets factor Spi-B. European Journal of Immunology. 2008; 38:2389–2400. [PubMed: 18792017]

48. Xiong H, et al. Ubiquitin-dependent degradation of interferon regulatory factor-8 mediated by Cbl down-regulates interleukin-12 expression. Journal of Biological Chemistry. 2005; 280:23531–23539. [PubMed: 15837792]

49. Edelson BT, et al. CD8a+ Dendritic Cells Are an Obligate Cellular Entry Point for Productive Infection by Listeria monocytogenes. Immunity. 2011; 35:236–248. [PubMed: 21867927]

50. Naik SH, et al. Cutting edge: generation of splenic CD8+ and CD8− dendritic cell equivalents in Fms-like tyrosine kinase 3 ligand bone marrow cultures. The Journal of Immunology. 2005; 174:6592–6597. [PubMed: 15905497]

51. Kanbe E, Zhang DE. A simple and quick method to concentrate MSCV retrovirus. Blood Cells Mol Dis. 2004; 33:64–67. [PubMed: 15223013]

52. Shooshtari P, et al. Correlation analysis of intracellular and secreted cytokines via the generalized integrated mean fluorescence intensity. Cytometry A. 2010; 77:873–880. [PubMed: 20629196]

53. Darrah PA, et al. Multifunctional TH1 cells define a correlate of vaccine-mediated protection against Leishmania major. Nat Med. 2007; 13:843–850. [PubMed: 17558415]

54. KCW, et al. L-Myc expression by dendritic cells is required for optimal T-cell priming. Nature. 2014

55. Langmead B, et al. Ultrafast and memory-efficient alignment of short DNA sequences to the human genome. Genome Biol. 2009; 10:R25. [PubMed: 19261174]

56. Li H, et al. The Sequence Alignment/Map format and SAMtools. Bioinformatics. 2009; 25:2078–2079. [PubMed: 19505943]

57. ENCODE Project Consortium. An integrated encyclopedia of DNA elements in the human genome. Nature. 2012; 489:57–74. [PubMed: 22955616]

58. Heinz S, et al. Simple combinations of lineage-determining transcription factors prime cis-regulatory elements required for macrophage and B cell identities. Mol Cell. 2010; 38:576–589. [PubMed: 20513432]

59. Zhang Y, et al. Model-based analysis of ChIP-Seq (MACS). Genome Biol. 2008; 9:R137. [PubMed: 18798982]

60. Bailey TL, et al. MEME SUITE: tools for motif discovery and searching. Nucleic Acids Res. 2009; 37:W202–W208. [PubMed: 19458158]

61. Loven J, et al. Selective inhibition of tumor oncogenes by disruption of super-enhancers. Cell. 2013; 153:320–334. [PubMed: 23582323]
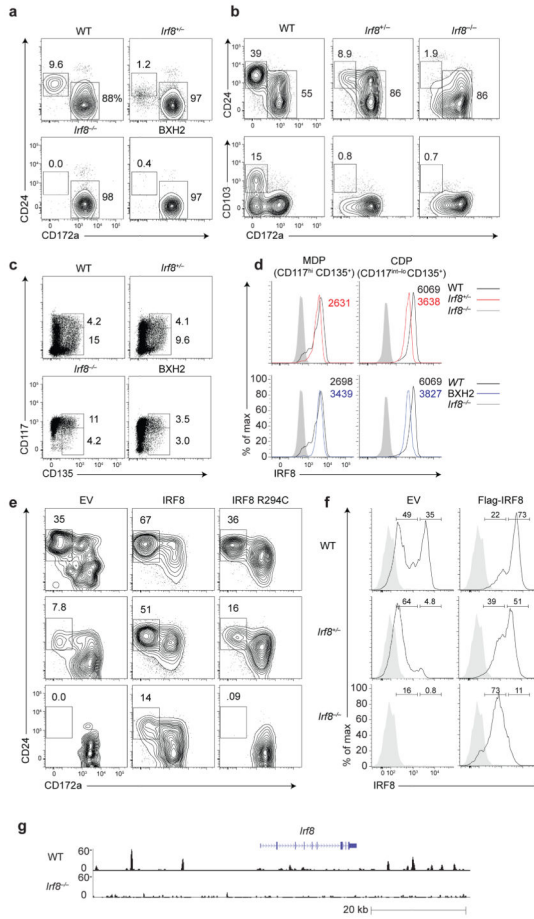
Figure 1.
IRF8 is regulated by PU.1-dependent autoactivation in the CDP. (**a**) Flow cytometry analysis of CD24$^+$ cDC frequency from live splenocytes in wild-type, $Irf8^{+/-}$, $Irf8^{-/-}$ or BXH2 mice. cDCs were gated as B220$^-$ SiglecH$^-$ CD11c$^+$ MHCII$^+$ (n=4–6). (**b**) Flow cytometry analyzing the expression of CD24, CD172a and CD103 in wild-type, $Irf8^{+/-}$ and $Irf8^{-/-}$ cDCs after 10 d of culture of BM with Flt3L. Numbers adjacent to outlined areas as in a (top row) or indicate percent CD103$^+$CD172a$^-$ cells (bottom row). (**c**) Flow cytometry of wild-type, $Irf8^{+/-}$, $Irf8^{-/-}$ or BXH2 BM, gated as Lin$^-$CD127$^-$CD115$^+$CD11c$^-$ (lineage (Lin) markers included CD11b, CD5, Gr-1, B220 and TER-119). Numbers adjacent to outlined areas indicate percent Lin$^-$ CD117^{hi}CD135$^+$ MDPs (top) or Lin$^-$ CD117^{int-lo}CD135$^+$ CDPs (bottom). (**d**) Flow cytometry analysis of IRF8 levels in MDPs and CDPs from mice of the indicated genotypes. Numbers show IRF8 MFI. Shaded histograms are $Irf8^{-/-}$ cells (n=2). (**e**) Flow cytometry analysis of CD24$^+$ CD172a$^-$ cDC development from wild-type, $Irf8^{+/-}$ and $Irf8^{-/-}$ BM cells, infected (GFP$^+$) with empty (EV), IRF8 or IRF8 R294C retrovirus, after 8 days of FLT3L culture (n=5). (**f**) Flow cytometry analysis of IRF8 expression in cDCs (CD11c$^+$ MHCII$^+$) in CD117^{hi} CD11b$^-$ wild-type, $Irf8^{+/-}$ and $Irf8^{-/-}$ BM cells, infected (GFP$^+$) with empty or Flag-tagged IRF8 retrovirus, after 8 days of FLT3L culture. The grey histogram represents background staining in IRF8$^{-/-}$ cDCs. Numbers indicate the percentage of cells in each gate (n=5).

Numbers indicates percentages of cells in each gate. (**g**) ChIP-seq analysis of IRF8 in DCs derived from wild-type or $Irf8^{-/-}$ BM cultured with FLT3L for 10 days.
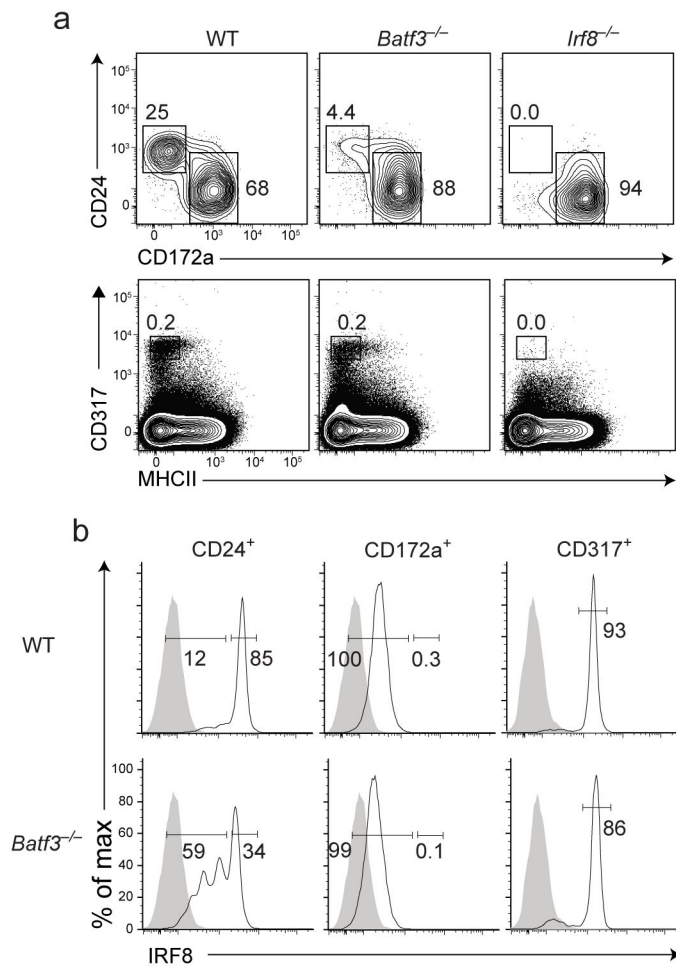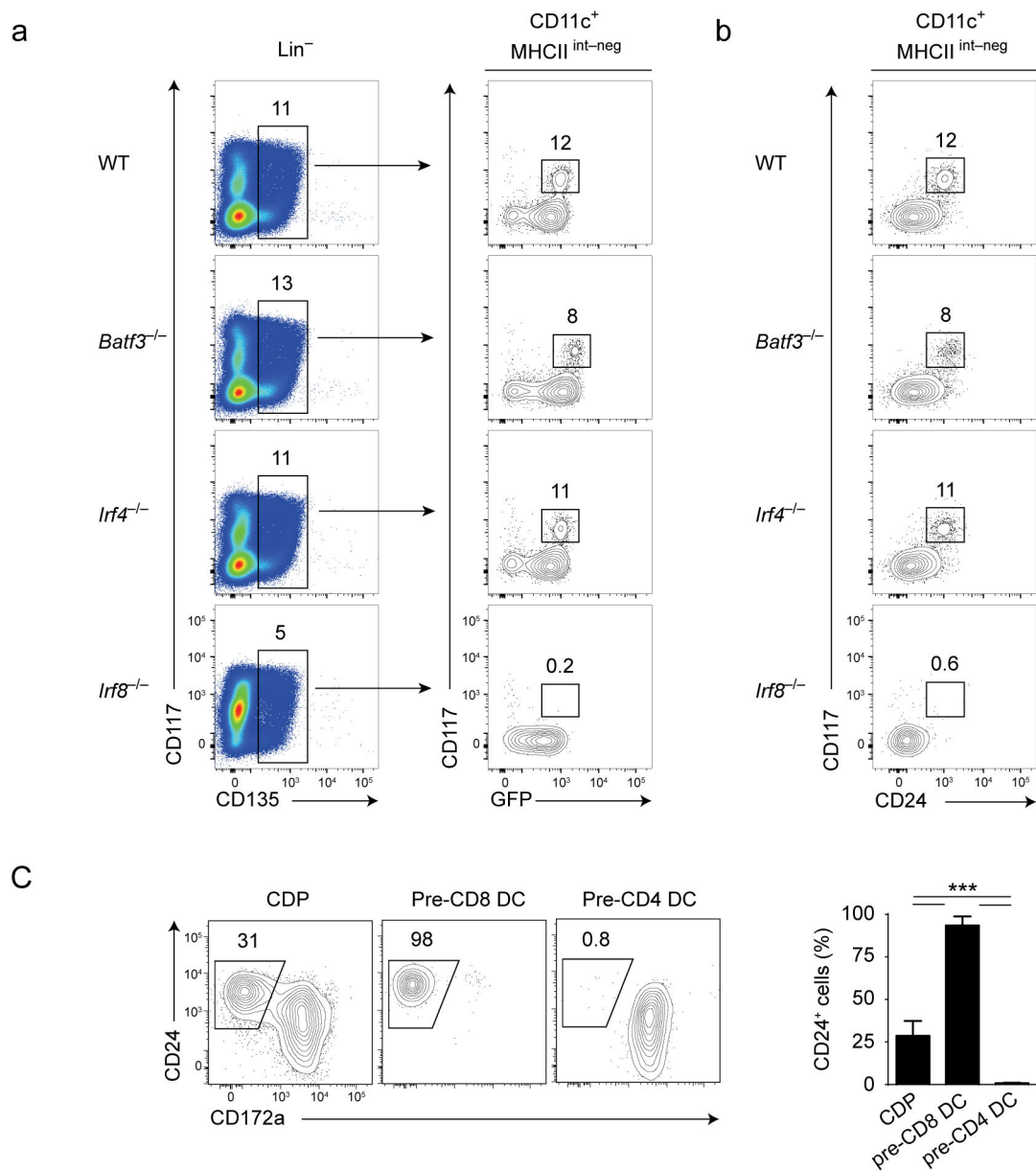
Figure 2.
Batf3 is required for IRF8 expression in CD8α+ cDCs. (**a**) Flow cytometry of fixed splenocytes from wild-type, *Batf3*−/− or *Irf8*−/− mice, with cDCs gated as B220−CD317−CD11c+MHCII+. Numbers adjacent to outlined areas indicate percent CD24+CD172a− cDCs (top left) or CD24−CD172a+ cDCs (bottom right) (top row), or CD317+MHCII− pDCs (bottom row). (**b**) Flow cytometry analysis of IRF8 expression in the indicated DC subsets from (**a**) was measured by ICS from wild-type and *Batf3*−/− mice (open histograms). Shaded histogram is background staining in *Irf8*−/− cells. Numbers are the percent of cells in IRF8lo and IRF8hi gates.
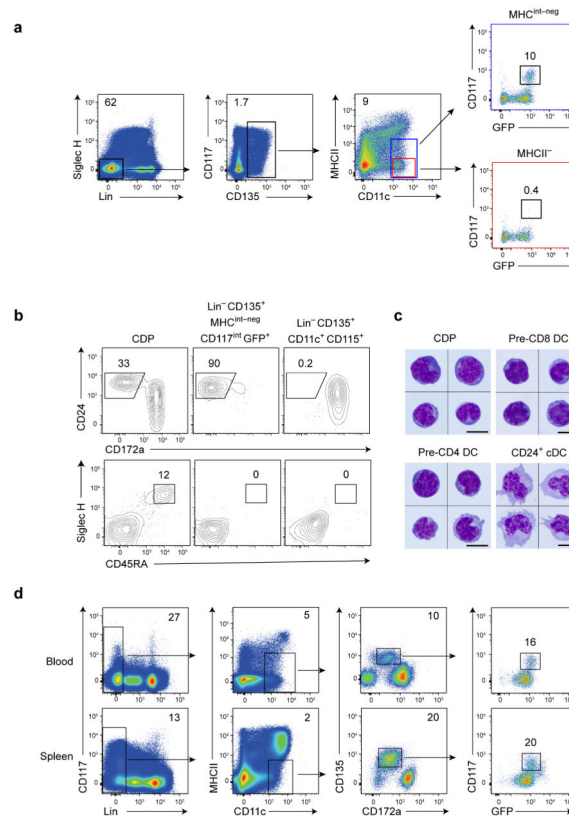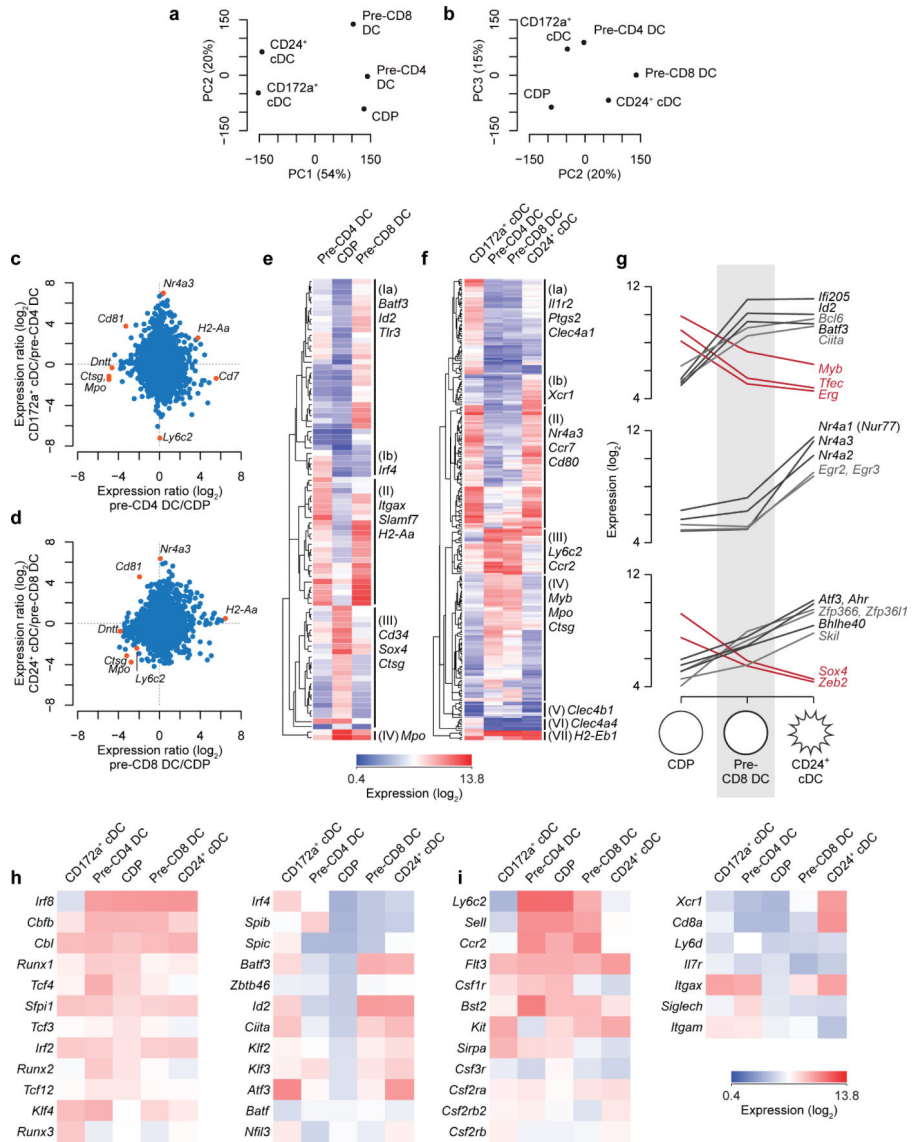
Figure 3.

Zbtb46 induction in CDPs identifies a clonogenic CD24^{+} cDC-committed progenitor in BM. (**a**) Flow cytometry analyzing the expression of GFP and CD117 (far right) in CD11c^{+}MHCII^{−} cells (bottom) or CD11c^{+}MHCII[int–neg] cells (top) among Lin^{−}Siglec-H^{−}CD135^{+} BM cells from *Zbtb46*[GFP/+] mice (*n* = 3); the lineage gate includes CD19, B220, CD3, NK1.1, CD105 and TER-119. Numbers in top left corners indicate percent Siglec-H^{−}Lin^{−} cells (far left) or CD135^{+} cells (middle left) or MHCII[int–neg]CD11c^{+} cells (blue); numbers above outlined areas (far right) indicate percent CD117^{int}GFP^{+} cells. (**b**) Flow cytometry analysis of CD24^{+} cDC, CD172a^{+} cDC or pDC development from BM CDPs, Siglec H^{−} CD117^{int} *Zbtb46*[GFP+] pre-cDCs, and CD117^{low} CD115^{+} pre-cDCs after a 4 day FlT3L culture (*n*=3). (**c**) Cells in (**b**) and splenic CD24^{+} cDCs were stained with Wright-Giemsa stain. Scale bars, 5 μm. (**d**) Flow cytometry of blood pre-cDCs (*n* = 2 samples from two mice each) and splenic pre-cDCs (Lin^{−}MHCII[int–lo]CD11c^{+}CD135^{+}CD172a^{int}) from *Zbtb46*[GFP/+] mice (*n* = 4); lineage markers include CD19, B220, CD3, NK1.1 and TER-119. Numbers in top right corners indicate percent Lin^{−} cells (far left), MHCII[int-neg]CD11c^{+} cells (middle left) or CD135^{+}CD172a^{int} cells (middle right); numbers above outlined areas (far right) indicate percent CD117^{int}GFP^{+} cells. Data are representative of three experiments (a,b), one experiment (c) or two experiments (d).
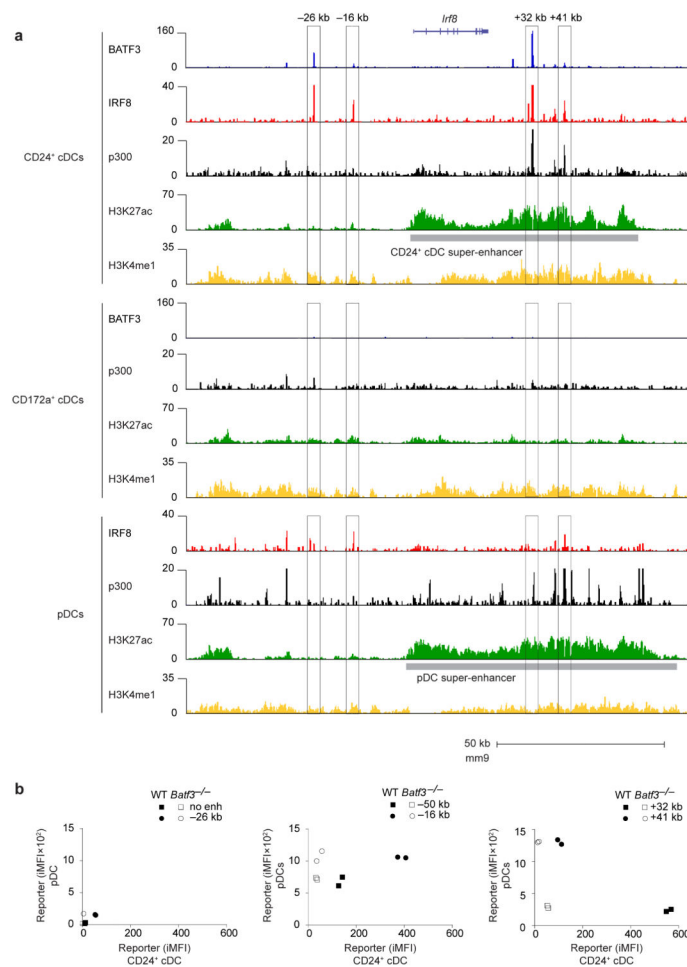
Figure 4.
Specification of pre-CD8 DCs requires IRF8 but not *Batf3*. (**a**) Flow cytometry analyzing the development of CD117^{int} *Zbtb46*-GFP$^+$ BM pre-CD8 DCs from *Zbtb46*$^{GFP/+}$ (WT), *Batf3*$^{-/-}$*Zbtb46*$^{GFP/+}$, *Irf4*$^{-/-}$*Zbtb46*$^{GFP/+}$ and *Irf8*$^{-/-}$ *Zbtb46*$^{GFP/+}$mice (*n* = 3 per genotype); lineage markers include CD19, B220, CD3, NK1.1, CD105 and TER-119. Numbers above outlined areas indicate percent CD135$^+$ cells (left) or CD117^{int}GFP$^+$ cells (right); above plots, pre-gating. (**b**) Flow cytometry analyzing the expression of CD24 in cells from a (*n* = 3 mice per genotype). Numbers above outlined areas indicate percent CD117$^+$CD24$^+$ cells. (**c**) Flow cytometry analyzing the development of CD24$^+$ cDCs (gated cells) and CD172a$^+$ cDCs (ungated cells) (left half) from cells purified by sorting of wild-type cells in b (middle), as well as CDPs (left) and pre-CD4 DCs (right), assessed after 5 d of culture with

Flt3L. Numbers above outlined areas (left) indicate percent $CD24^+CD172a^-$ cells. Right, frequency of $CD24^+$ cells that developed from the progenitors at left ($n = 7$ mice). *$P <$ 0.001 (one-way analysis of variance (ANOVA) with Tukey's post-hoc test). Data are representative of two experiments (a,b) or three experiments (c; average and s.e.m.).

Figure 5.
Pre-CD8 DCs are a distinct development stage from the CDP and mature CD24+ cDCs.
(**a,b**) Principal component analysis of indicated populations showing segregation by
developmental stage (PC1) and by lineage (PC2 and PC3). Percents in parentheses indicate
proportion of variance explained. (**c, d**) Pairwise comparisons of gene expression ratios,
showing ratios between committed progenitors and CDPs on the horizontal axis and
between mature cDCs and their committed progenitors on the vertical axis. Each dot
indicates an individual probe set. (**e, f**) Hierarchical clustering of genes expressed at least
eight fold differently between the committed progenitors and the CDP (**e**) or between the
committed progenitors and their corresponding mature cDC subsets (**f**). (**g**) Shown is the
relative expression of all transcription factor-encoding genes differing by at least eightfold
between the CDP and CD24+ cDCs. (**h, i**) Relative expression is shown for the indicated
transcription factors (**h**) or cell surface markers (**i**) in the indicated populations.

Figure 6.
A Batf3-dependent *Irf8* enhancer functions selectively in CD24+ cDCs. (**a**) ChIP-Seq was performed for Batf3, IRF8, p300, H3K27ac and H3K4me1 in sort-purified CD24+ cDCs, for Batf3, p300, H3K27ac and H3Kme1 in sort purified CD172a+ cDCs and for IRF8, p300, H3K27ac and H3Kme1 in sort purified pDCs. Boxes at −26 kb, −16 kb, +32 kb and +41 kb relative to the *Irf8* TSS indicate regions were tested for enhancer activity. The PU.1 binding element at −50 kb[44] is not shown. (**b**) Retroviral reporter constructs containing the indicated enhancer elements identified in (**a**) were transduced into BM cells enriched for CD117 expression, cultured with FLT3L and analyzed after 7 days for reporter activity. Shown are integrated MFI (see methods) for each reporter in duplicate for pDCs and CD24+ cDCs as gated in Supplementary Fig. 4 i–j.
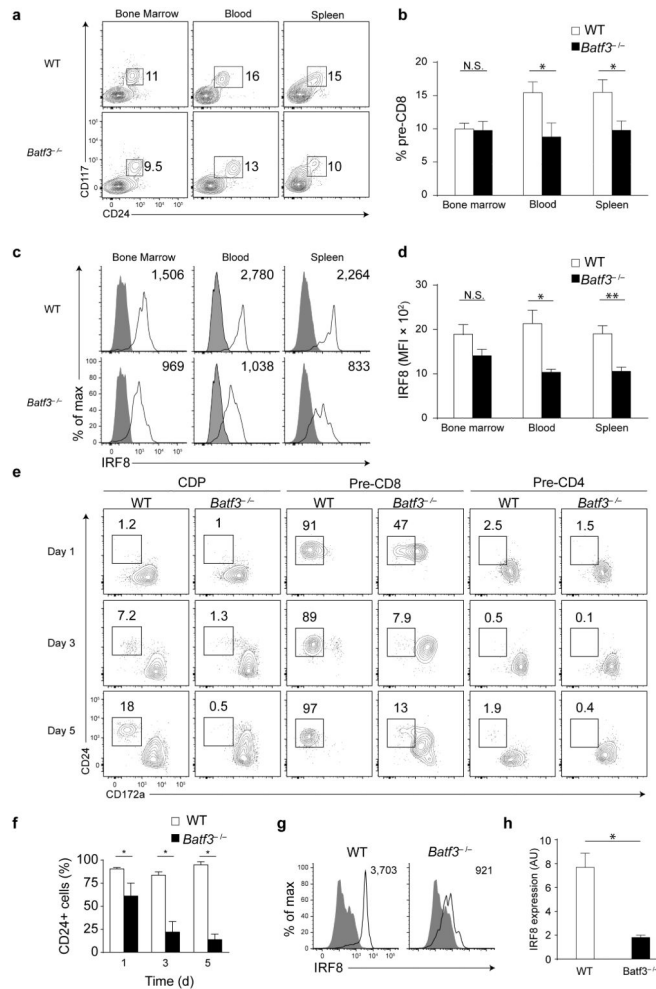
Figure 7.
Specified pre-CD8 DCs are diverted to the CD172a+ lineage in the absence of Batf3. (**a**)
Flow cytometry analysis of pre-CD8 DC frequency among pre-cDCs in BM (*n*=7), blood
(*n*=5) and spleen (*n*=6) from wild-type and *Batf3*−/− mice. Numbers indicate percentage. (**b**)
Average frequency of pre-CD8 DCs from (**a**), unpaired *t*-test, error bars indicate s.e.m. (**c**)
Flow cytometry analysis of IRF8 expression in pre-CD8 DCs from BM (*n*=7), blood (*n*=5)
and spleen (*n*=6) in wild-type and *Batf3*−/− mice (solid line). Numbers indicate geometric
MFI of IRF8 expression. Background IRF8 levels (shaded) are shown for CD24− cDCs of
each tissue. (**d**) Average geometric MFI of IRF8 expression in pre-CD8 DCs from (**c**),
unpaired *t*-test performed for BM and spleen, unpaired *t*-test with Welch's correction
performed for blood, error bars indicate s.e.m. (**e**) Flow cytometry analysis of CD24+ cDC
and CD172a+ cDC development from CDPs, pre-CD8 DCs and pre-CD4 DCs from wild-
type or *Batf3*−/− mice cultured with Flt3L and CD45.1 BM cells after 1, 3 and 5 days, (*n*=4),
numbers indicate percentage. (**f**) Average percentage of CD24+ cDCs from cells in (**e**),
(*n*=4), Mann-Whitney test. (**g**) Flow cytometry analysis of IRF8 expression in pre-CD8 DCs
(solid line) from wild-type (*n*=4) and *Batf3*−/− (*n*=4) mice after 5 days of FLT3L culture.
Shaded histogram represents IRF8 expression in CD172a+ cDCs developed form CDPs after

5 days. (**h**) Average IRF8 expression from cells in (**g**), Mann-Whitney test. * $P < 0.05$, ** $P < 0.01$.
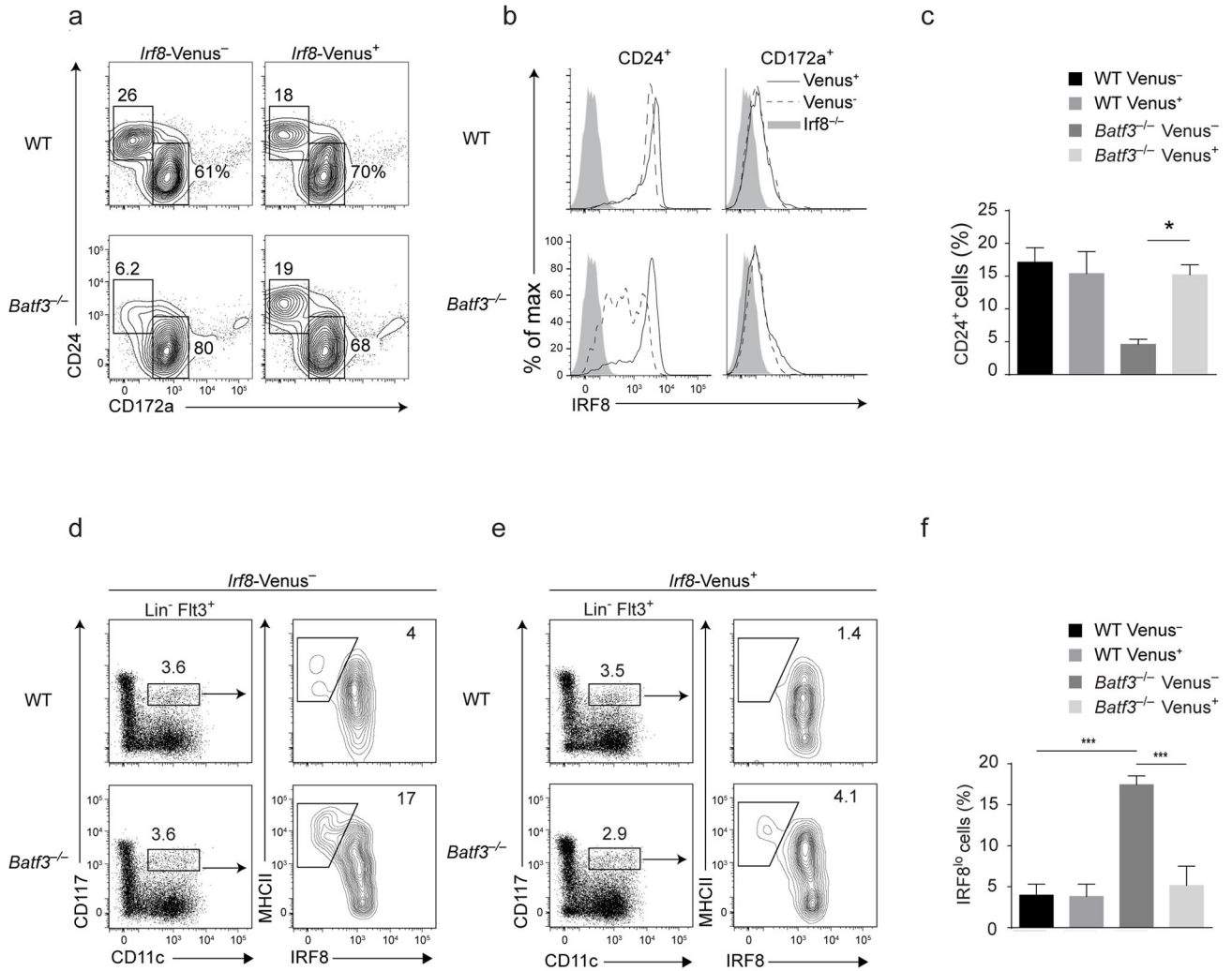
Figure 8.
Transgenic IRF8 overexpression bypasses the Batf3 requirement in CD8α⁺ cDC development. (**a**) Flow cytometry analysis of CD24⁺ cDC and CD172a⁺ cDC frequency in splenocytes from wild-type, *Batf3*⁻/⁻, *Irf8*^VENUS+, and *Batf3*⁻/⁻ *Irf8*^VENUS+ mice. Data are representative of 6–8 mice per genotype. Numbers indicate the percent of cells in each gate. (**b**) Flow cytometry analysis of IRF8 expression in CD24⁺ and CD172a⁺ cDCs from (**a**) from wild-type and *Batf3*⁻/⁻ mice (dashed lines) or *Irf8*^VENUS+ and *Batf3*⁻/⁻ *Irf8*^VENUS+ mice (solid lines). Background IRF8 staining (shaded) is shown for *Irf8*⁻/⁻ splenocytes. (**c**) Average frequency of CD24⁺ cDCs as a percentage of cDCs from the indicated genotypes, *n*=7–8 mice per genotype, one-way ANOVA, Tukey's post-hoc test, error bar indicates s.e.m. (**d, e**) Flow cytometry analysis of IRF8 and MHCII levels in Lin⁻ Flt3⁺ CD117^int BM cells from mice in (**a**). Lin includes CD19, B220, CD3, NK1.1, CD105, TER-119 (*n*=6). (**f**) Average frequency of MHCII^high IRF8^low cells as percentage of Lin⁻ Flt3⁺ CD117^int BM cells from mice in (**a**), n=6, one-way ANOVA, Tukey's post-hoc test, error bar indicates s.e.m. *$P < 0.05$, ***$P < 0.001$.